THE AMERICAN SOCIETY OF MECHANICAL ENGINEERS
345 E. 47th St., New York, N.Y. 10017

94-GT-200

MODELING FOR CONTROL OF ROTATING STALL IN HIGH SPEED MULTI-STAGE AXIAL COMPRESSORS

Matthew R. Feulner
Dept. of Aeronautics and Astronautics
Massachusetts Institute of Technology
Cambridge, Massachusetts

Gavin J. Hendricks
United Tech. Research Center
East Hartford, Connecticut

James D. Paduano
Department of Aeronautics and Astronautics
Massachusetts Institute of Technology
Cambridge, Massachusetts

ABSTRACT

Using a two dimensional compressible flow representation of axial compressor dynamics, a control-theoretic input-output model is derived which is of general utility in rotating stall/surge active control studies. The derivation presented here begins with a review of the fluid dynamic model, which is a 2D stage stacking technique that accounts for blade row pressure rise, loss and deviation as well as blade row and inter-blade row compressible flow. This model is extended to include the effects of the upstream and downstream geometry and boundary conditions, and then manipulated into a transfer function form that dynamically relates actuator motion to sensor measurements. Key relationships in this input-output form are then approximated using rational polynomials. Further manipulation yields an approximate model which is in standard form for studying active control of rotating stall and surge. As an example of high current relevance, the transfer function from an array of jet actuators to an array of static pressure sensors is derived. Numerical examples are also presented, including a demonstration of the importance of proper choice of sensor and actuator locations, as well as a comparison between sensor types. Under a variety of conditions, it was found that sensor locations near the front of the compressor or in the downstream gap are consistently the best choices, based on a quadratic optimization criterion and a specific 3-stage compressor model. The modeling and evaluation procedures presented here are a first step toward a rigorous approach to the design of active control systems for high speed axial compressors.

Nomenclature

a	sound speed
j	$\sqrt{-1}$
r	rotor radius
s	Laplace variable
t	time
x	axial coordinate
x'	blade row coordinate
M	Mach number
P	pressure
S	entropy
V	velocity
W	velocity in blade row
γ	specific heat ratio
ρ	density
θ	circumferential coordinate
ξ	blade stagger
τ	time constant
Ω	rotor angular frequency
$\delta\beta$	deviation

Subscripts and Superscripts

k	blade row or gap number
ka	gap location of actuator
ks	gap location of sensor
n	Fourier harmonic number
K	total number of blade rows
SS	steady state
T	complex conjugate transpose

PDE Solution Matrices and Vectors

$\mathbf{b}^1$	jet actuator matrix (Eqn 12)
$\mathbf{v}$	vector of gap unknowns (Eqn 4)
$\tilde{\mathbf{v}}$	vector of blade row unknowns (Eqn 2)
$\mathbf{A}$	transmission matrix (Eqns 9 and 10)
$\mathbf{B}$	blade row solution matrix (Eqn 2)
$\mathbf{B}_L$, $\mathbf{B}_T{}^1$	boundary conditions matrices (Eqns 5 and 6)
$\mathbf{D}^1$	deviation matrix (Eqn 6)
$\mathbf{J}^1$	jet actuator matrix (Eqn 12)
$\mathbf{N}$	inlet condition matrix (Eqn 7)
$\mathbf{P}^1$	total pressure loss matrix (Eqn 5)

[1] Indicates matrices whose entries are linearization constants.

Presented at the International Gas Turbine and Aeroengine Congress and Exposition
The Hague, Netherlands — June 13–16, 1994
This paper has been accepted for publication in the Transactions of the ASME
Discussion of it will be accepted at ASME Headquarters until September 30, 1994

S^1 sensor matrix (Eqn 13)
V gap solution matrix (Eqn 4)
V_L, V_T^1 boundary conditions matrices (Eqns 5 and 6)
X exit condition matrix (Eqn 8)

LQG Matrices and Vectors

x state vector (Eqn 19)
A state weighting matrix (Eqn 20)
B control weighting matrix (Eqn 20)
C optimal regulator gain (Eqn 20)
F, G, H, D state space representation matrices (Eqn 19)
P solution to estimation Riccati equation (Eqn 20)
Q process noise covariance (Eqn 20)
R measurement noise covariance
S solution to control Riccati equation (Eqn 20)

Acronyms

LQG Linear Quadratic Gaussian
IGV Inlet Guide Vanes

1 INTRODUCTION

Considerable work has been done in recent years on modeling and controlling rotating stall and surge in axial compressors (see the review Greitzer et al., 1992). In each of these studies, assumptions concerning the compressor operating characteristics are made, which are deemed consistent with the experimental apparatus of interest. As the technology of rotating stall and surge control becomes more advanced, and as the experiments conducted to verify the concepts become more sophisticated and realistic, the number of assumptions that can be maintained diminishes.

For example, early proof-of-concept studies in surge control (Ffowcs-Williams and Huang, 1989, Pinsley et al., 1991) assumed one-dimensional flow through the compression system. In axial compressors, however, the 1D assumption is often not tenable; rotating stall instabilities are fundamentally (at least) two-dimensional. Thus rotating stall control studies (Epstein et al., 1989, Paduano et al., 1993, Haynes et al., 1993) required 2D models to motivate control system configuration and controller design. Demonstrations of rotating stall stabilization were conducted on low-speed compressors that exhibited behavior which was well described by linear incompressible theory; thus the assumptions of linearity and incompressibility proved to be valid for the purpose of stabilization and range extension by active control.

In high-speed compressors, which are the focus of current research, both nonlinearity and compressibility must be addressed. Nonlinear modeling of rotating stall and surge has been studied by various authors (Greitzer, 1976, McCaughan, 1989ab, Adomaitis and Abed, 1993, Badmus et al., 1993, Mansoux et al., 1994), and may prove important to the success of stabilization efforts. Compressible modeling of the 2D process, on the other hand, has received much less attention. To our knowledge, the only work on this problem has been by Bonnaure (1991) and Hendricks et al. (1993), who describe a rigorous 2D, linearized, compressible analysis, which we will take as our starting point. Note that in this analysis the linearity assumption is maintained, which allows the circumferential perturbation at any axial station to be represented as a sum of sinusoidal harmonics (Paduano et al., 1990). Each harmonic perturbation develops independently in the linearized analysis, which allows modeling to be done on each circumferential harmonic separately.

In this paper, the fluid dynamic model developed by Bonnaure (1991) and Hendricks et al. (1993) is reviewed, modified, and augmented in the context of active control. Two primary steps are necessary to convert the model to one useful for active control. First, the model must be augmented to include the effects of actuator motion. The result of this process is an input-output form in the frequency (Laplace transform) domain. This form is important for control law analysis as well as for a basic understanding of the behavior of an actuated compressor.

Second, and perhaps more challenging, is the necessity to convert the model to a form that is a rational polynomial in the Laplace transform variable s. This form is essential for control system analysis and design: rational polynomial representations are equivalent to (and routinely converted to) state-space representations, which are used in virtually every modern computational procedure for control system analysis and synthesis.

The source of irrational, or transcendental, transfer functions in axial compressors is compressibility. To understand this, first consider the incompressible case: it has been shown both theoretically (Moore and Greitzer, 1986, Longley, 1993) and experimentally (Paduano et al., 1993, Haynes et al., 1993) that, in low speed compressors, a finite number of eigenvalues (typically 1 to 3) can be used to completely describe the dynamic evolution of *each circumferential harmonic* of the flow perturbation. This is true because, in incompressible flow, the axial dimension of the compressor can be 'solved out' of the system dynamics. When modeling compressibility, however, one introduces such effects as acoustic and convection time delays in the axial direction. The resulting dynamics are infinite-dimensional (i.e. distributed) for each harmonic of the perturbation, reflecting the fact that flow variables can vary dynamically with axial distance along the duct. Similar effects occur in acoustic ducts (Takahashi et al., 1972), whose transfer functions (often called 'transmission matrices') are transcendental functions of s.

Fortunately, arbitrarily accurate rational polynomial approximations to irrational transfer functions can be made. For high speed compressors, however, this is by no means a trivial exercise, and thus model conversion constitutes the primary contribution of this paper. Eigenvalue locations and open loop Bode plots are used to verify the approximations, and to compare the rational polynomial model to the analytical model.

The paper is organized as follows: Section 2 presents the fluid dynamics, and Section 3 describes conversion to input-output, and then rational polynomial, form. In Section 4, the rational approximate model is verified against the exact model, and several example applications are given. These examples demonstrate the model developed is useful for control system design studies in high speed multi-stage compressors.

2 REVIEW OF THE COMPRESSIBLE MODEL

2.1 Basic Equations

The 2D compressible model is composed of 1D blade row models and 2D inter-blade row gap models, which are 'stacked up' axially through the compressor using boundary conditions at each interface and closed by end conditions at the inlet and exit of the compressor ducts (see Figure 1). Each equation is decomposed using a complex Fourier series around the annulus

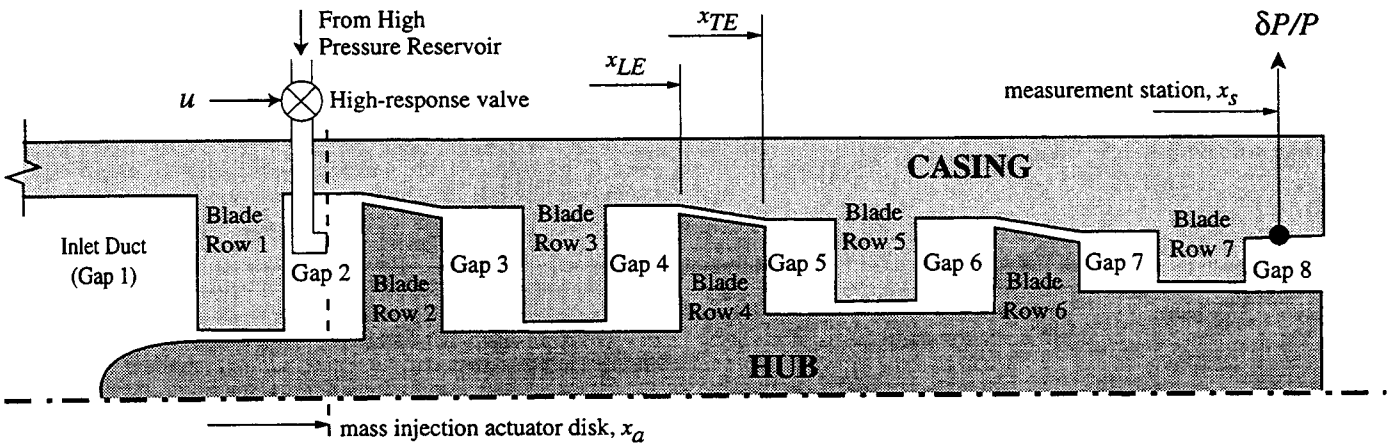

Figure 1 - Numbering of gap blade rows for stacking procedure, for a 3-stage compressor with inlet guide vanes. In this example, K=7, ka=2, and ks=8.

which results in independent solutions for each circumferential harmonic (for details of modeling compressor dynamics with Fourier harmonics, see Paduano et al., 1990).

The blade rows are assumed to be a set of parallel one dimensional passages with no circumferential cross flow. The 1D flow equations linearized about the operating point are a set of constant coefficient equations:

Mass Continuity Equation:

$$\frac{\partial \delta\rho}{\partial t} + W\frac{\partial \delta\rho}{\partial x'} = -\rho\frac{\partial \delta W}{\partial x'}$$

Momentum Equation:

$$\frac{\partial \delta W}{\partial t} + W\frac{\partial \delta W}{\partial x'} = -\frac{1}{\rho}\frac{\partial \delta P}{\partial x'}$$

Energy Equation (for a perfect gas):

$$\frac{\partial \delta P}{\partial t} + W\frac{\partial \delta P}{\partial x'} = a^2\left(\frac{\partial \delta\rho}{\partial t} + W\frac{\partial \delta\rho}{\partial x'}\right)$$

where $x' = x/\cos\xi$ (ξ is the blade stagger angle). These equations can be manipulated into a wave equation in static pressure for the fluid in the blade row reference frame:

$$\left(\frac{\partial}{\partial t} + W\frac{\partial}{\partial x'}\right)^2 \delta P = a^2\frac{\partial^2}{\partial x'^2}\delta P.$$

Since the equations are linear, they can be solved by Fourier superposition; thus solutions of the form $\delta P = \sum_n A(n,x,s)e^{j(\omega+n\Omega)t}e^{jn\theta}$ are sought, where $A(n,x,s)$ is to be solved by substitution, and Ω is the rotor angular rate (solutions are in the stationary reference frame). Bonnaure (1991) carried out the substitution and found the following solutions:

$$\begin{aligned}
\frac{\delta P}{P}(x,\theta,s) &= \gamma\sum_{n=-\infty}^{\infty}\left[\tilde{B}_n(s)e^{\tilde{\alpha}_n(s)x} + \tilde{C}_n(s)e^{\tilde{\beta}_n(s)x}\right]e^{jn\theta} \\
\frac{\delta\rho}{\rho}(x,\theta,s) &= \sum_{n=-\infty}^{\infty}\left[\tilde{B}_n(s)e^{\tilde{\alpha}_n(s)x} + \tilde{C}_n(s)e^{\tilde{\beta}_n(s)x} + \tilde{E}_n(s)e^{\tilde{\chi}_n(s)x}\right]e^{jn\theta} \qquad (1) \\
\frac{\delta W}{a}(x,\theta,s) &= \sum_{n=-\infty}^{\infty}\left[-\tilde{B}_n(s)e^{\tilde{\alpha}_n(s)x} + \tilde{C}_n(s)e^{\tilde{\beta}_n(s)x}\right]e^{jn\theta}
\end{aligned}$$

where the time part of the solutions has been Laplace transformed ($s=j\omega$) for use in later developments, and

$$\begin{aligned}
\tilde{\alpha}_n(s) &= \frac{1}{\cos\xi}\left(-\frac{jn}{r}\sin\xi + \frac{s+jn\Omega}{a-W}\right) \\
\tilde{\beta}_n(s) &= \frac{1}{\cos\xi}\left(-\frac{jn}{r}\sin\xi - \frac{s+jn\Omega}{a+W}\right) \\
\tilde{\chi}_n(s) &= \frac{1}{\cos\xi}\left(-\frac{jn}{r}\sin\xi - \frac{s+jn\Omega}{W}\right)
\end{aligned}$$

r is the rotor radius, ξ is the blade stagger angle, a is the local sound velocity, n is the circumferential harmonic number, and s is the Laplace transform variable. $\tilde{B}$ and $\tilde{C}$ represent upstream and downstream traveling static pressure perturbations respectively, and $\tilde{E}$ represents entropy perturbations, which travel with the fluid velocity.

The solutions (1) are combinations of the functions $e^{\tilde{\alpha}_n(s)x}$, $e^{\tilde{\beta}_n(s)x}$, and $e^{\tilde{\chi}_n(s)x}$, which are the Laplace transforms of the various transport time delays across the blade row: $e^{\tilde{\alpha}_n(s)x}$ represents the transport time of upstream traveling pressure perturbations, $e^{\tilde{\beta}_n(s)x}$ represents the transport time of downstream traveling pressure perturbations, and $e^{\tilde{\chi}_n(s)x}$ represents the convection time of the downstream

traveling entropy perturbation. The time (or s) dependence of the amplitude of each perturbation mode ($\tilde{B}$, $\tilde{C}$, and $\tilde{E}$ for the blade row) remains to be solved, as an eigenvalue problem in s, once all blade rows and gaps are interconnected.

A more compact way to write these equations is using a vector-matrix form:

$$\begin{bmatrix} \frac{\delta P}{P} \\ \frac{\delta \rho}{\rho} \\ \frac{\delta W}{a} \end{bmatrix}(x,\theta,s) = \sum_n e^{jn\theta}\mathbf{B}_n(x,s)\begin{bmatrix} \tilde{B}_n \\ \tilde{C}_n \\ \tilde{E}_n \end{bmatrix}(s) = \sum_n e^{jn\theta}\mathbf{B}_n(x,s)\tilde{\mathbf{v}}_n(s) \tag{2}$$

where $\mathbf{B}_n(x,s)$ is a matrix containing all of the 'known' parts of the solution, and $\tilde{\mathbf{v}}_n(s)$ is a vector of perturbation magnitudes which are as yet unknown. The matrix form facilitates stage stacking, as well as manipulation of the equations into transfer function form; both procedures will be discussed below.

The inter-blade row gap and duct equations are similarly linearized and solved through the Laplace transform in time and a complex Fourier series in circumferential position. The 2D solutions are (Bonnaure, 1991):

$$\begin{aligned}
\frac{\delta P}{P}(x,\theta,s) &= \sum_{n=-\infty}^{\infty}\gamma\left[\left(r\alpha_n(s)M_x+\left(\frac{sr}{a}+jnM_\theta\right)\right)B_n(s)e^{\alpha_n(s)x}+\left(r\beta_n(s)M_x+\left(\frac{sr}{a}+jnM_\theta\right)\right)C_n(s)e^{\beta_n(s)x}\right]e^{jn\theta}\\
\frac{\delta \rho}{\rho}(x,\theta,s) &= \sum_{n=-\infty}^{\infty}\left[\left(r\alpha_n(s)M_x+\left(\frac{sr}{a}+jnM_\theta\right)\right)B_n(s)e^{\alpha_n(s)x}+\left(r\beta_n(s)M_x+\left(\frac{sr}{a}+jnM_\theta\right)\right)C_n(s)e^{\beta_n(s)x}+E_n(s)e^{\chi_n(s)x}\right]e^{jn\theta}\\
\frac{\delta V_x}{a}(x,\theta,s) &= \sum_{n=-\infty}^{\infty}\left[-r\alpha_n(s)B_n(s)e^{\alpha_n(s)x}-r\beta_n(s)C_n(s)e^{\beta_n(s)x}+jnM_xD_n(s)e^{\chi_n(s)x}\right]e^{jn\theta}\\
\frac{\delta V_\theta}{a}(x,\theta,s) &= \sum_{n=-\infty}^{\infty}\left[-jnB_n(s)e^{\alpha_n(s)x}-jnC_n(s)e^{\beta_n(s)x}+\left(\frac{sr}{a}+jnM_\theta\right)D_n(s)e^{\chi_n(s)x}\right]e^{jn\theta}
\end{aligned} \tag{3}$$

or, more compactly,

$$\begin{bmatrix} \frac{\delta P}{P} \\ \frac{\delta \rho}{\rho} \\ \frac{\delta V_x}{a} \\ \frac{\delta V_\theta}{a} \end{bmatrix}(x,\theta,s) = \sum_n e^{jn\theta}\mathbf{V}_n(x,s)\begin{bmatrix} B_n \\ C_n \\ D_n \\ E_n \end{bmatrix}(s) = \sum_n e^{jn\theta}\mathbf{V}_n(x,s)\mathbf{v}_n(s) \tag{4}$$

where

$$\alpha_n(s),\beta_n(s) = \frac{M_x\left(\frac{sr}{a}+jnM_\theta\right)\pm\sqrt{n^2\left(1-M_x^2\right)+\left(\frac{sr}{a}+jnM_\theta\right)^2}}{r\left(1-M_x^2\right)}$$

$$\chi_n(s) = -\frac{\frac{sr}{a}+jnM_\theta}{rM_x}$$

M_x and M_θ are the axial and circumferential Mach numbers, B and C represent static pressure perturbations, and D and E represent vorticity and entropy perturbations, respectively.

Note that in our representation, each circumferential Fourier harmonic $e^{jn\theta}$ is an independent entity. Thus a complete model of the compressor dynamics consists of a set of independent models, each of which describes the dynamic evolution of one such harmonic. Experimental and theoretical results indicate that the first three such harmonics (n=1,2, and 3) are the most unstable and thus the most important for stability and control studies.

Although the *circumferential* space dimension is heretofore 'solved out' of the dynamic equations by the decoupling of the harmonics, *axial* variations in the flow variables are not as easily represented. In fact, the form of equations (1) and (3) yields an infinity of eigenvalues, which represent the axial continuum of flow variations. The simplification of this axial representation of the dynamics will be presented in Section 3.2.

All dependencies on the circumferential harmonic number, n, will be dropped throughout the rest of the paper for notational convenience.

2.2 Boundary Conditions

At each leading and trailing edge of a blade row, boundary conditions must be used to connect the solutions of the blade row to that of the gap or duct. The leading edge boundary conditions are continuity, relative total temperature conservation, and a relative total pressure loss characterized by a loss coefficient and a time lag. The trailing edge boundary conditions are continuity, relative total temperature conservation, relative total pressure conservation and a deviation characterized by a deviation coefficient and a time lag. In terms of equations (2) and (4) these conditions (Bonnaure, 1991) can also be written in vector-matrix form:

Leading edge:

$$\mathbf{B}_{Lk}\mathbf{B}_k(x_{LEk},s)\tilde{\mathbf{v}}_k(s) = \left(\mathbf{V}_{Lk}+\frac{1}{1+s\tau}\mathbf{P}_k\right)\mathbf{V}_k(x_{LEk},s)\mathbf{v}_k(s) \tag{5}$$

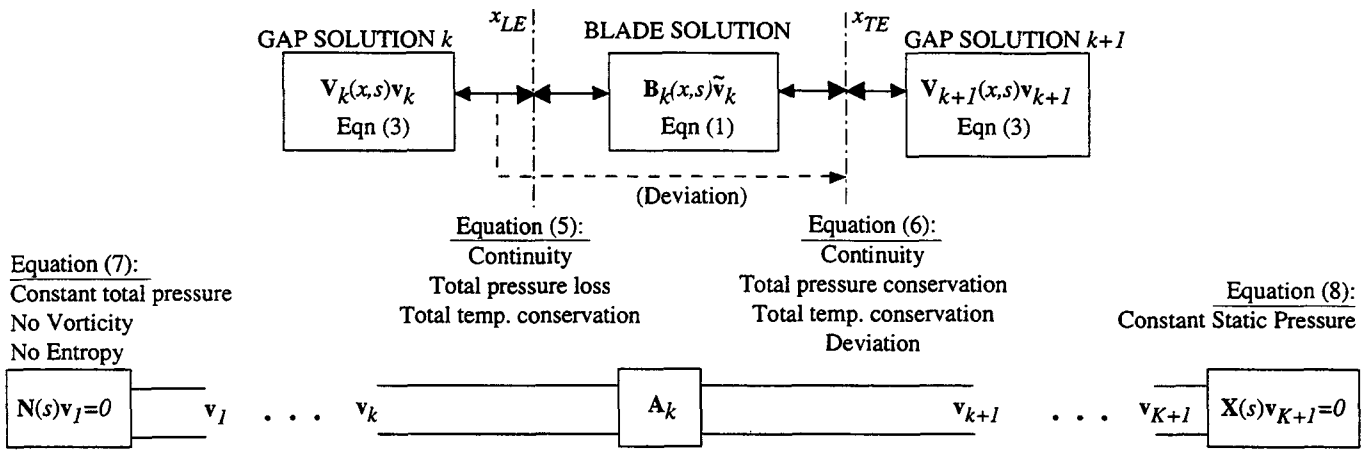

Figure 2 - Schematic of interconnections used to build system matrices. Each blade row+gap is represented by a transmission matrix $\mathbf{A}_k(s)$. Combining $\mathbf{A}_k$'s and closing with boundary conditions gives homogeneous dynamics.

Trailing edge:

$$\mathbf{V}_{Tk+1}\mathbf{V}_{k+1}(x_{TEk},s)\mathbf{v}_{k+1}(s) = \mathbf{B}_{Tk}\mathbf{B}_k(x_{TEk},s)\tilde{\mathbf{v}}_k(s) - \frac{1}{1+s\tau}\mathbf{D}_k\mathbf{V}_k(x_{LEk},s)\mathbf{v}_k(s) \quad (6)$$

where each equation is a matrix representation of the respective boundary equations (note that $\tilde{\mathbf{v}}_k(s)$ and $\mathbf{v}_k(s)$ appear in each), and the subscript k denotes the blade row or gap number. The numbering scheme for blades, gaps, and ducts is shown in Figure 1 and used throughout. Equations (2) and (4) serve to define $\mathbf{B}_k(x,s), \mathbf{V}_k(x,s), \tilde{\mathbf{v}}_k$, and $\mathbf{v}_k$ for the kth blade or gap; $\mathbf{B}_{Lk}, \mathbf{V}_{Lk}, \mathbf{P}_k, \mathbf{B}_{Tk}, \mathbf{V}_{Tk}$, and $\mathbf{D}_k$ contain the (*s-independent*) coefficients which result when the boundary conditions are linearized about the mean flow. The latter matrices allow one to incorporate the following characteristics for each blade row: the pressure rise coefficient (i.e. the slope of the pressure rise-mass flow characteristic), and the loss and deviation coefficients. We omit both the boundary condition equations and the detailed expansions of the coefficient matrices here for brevity.

End conditions are also required at the upstream end of the upstream duct and at the downstream end of the downstream duct (these ducts are represented using the gap equations (3)). The end conditions depend on the compressor installation to be modeled. At the entrance to the inlet duct, we assume that total pressure is constant, and entropy and vorticity are zero. This corresponds to clean inlet conditions during an open-circuit compressor test. At the exit of the downstream duct, we assume that static pressure is constant, which models the case where the flow dumps into a plenum. These conditions can be written in vector-matrix form as well:

Upstream:

$$\begin{bmatrix} \delta(\textit{total pressure}) \\ \delta(\textit{entropy}) \\ \delta(\textit{vorticity}) \end{bmatrix} = \begin{bmatrix} 0 \\ 0 \\ 0 \end{bmatrix} \quad \Rightarrow \quad \mathbf{N}(s)\mathbf{v}_1(s) = \begin{bmatrix} 0 \\ 0 \\ 0 \end{bmatrix} \quad (7)$$

Downstream:

$$\frac{\delta P}{P} = 0 \quad \Rightarrow \quad \mathbf{X}(s)\mathbf{v}_{K+1}(s) = 0 \quad (8)$$

where $\mathbf{X}(s)$ and $\mathbf{N}(s)$ are matrices containing the linearized end conditions combined with equation (4). These boundary conditions are modifications to those used by Bonnaure (1991), and are considered to be more realistic.

2.3 Solution

The overall solution can be obtained by "stacking" the solutions across each blade row and applying the end conditions. Figure 2 shows the way that the boundary conditions and end conditions inter-relate to form the overall dynamic system. Across each blade row, the transformation is expressed as:

$$\mathbf{v}_{k+1}(s) = \mathbf{A}_k(s)\mathbf{v}_k(s) \quad (9)$$

where $\mathbf{A}_k(s)$ is obtained by eliminating $\tilde{\mathbf{v}}_k(s)$ from equations (5) and (6), and solving for $\mathbf{v}_{k+1}(s)$ in terms of $\mathbf{v}_k(s)$. Note that equations (5) and (6) use the transformations $\mathbf{B}_k(x,s)$ and $\mathbf{V}_k(x,s)$, which represent the dynamics of the blades and gaps respectively. Thus $\mathbf{A}_k(s)$ represents all of the dynamics from the leading edge of blade row k to the leading edge of blade row k+1. Stacking each of these transformations as in Figure 2 results in an expression relating the inlet and exit duct solutions:

$$\mathbf{v}_{K+1}(s) = \mathbf{A}_K(s)\cdots\mathbf{A}_1(s)\mathbf{v}_1(s) = \mathbf{A}(s)\mathbf{v}_1(s) \quad (10)$$

Applying the end conditions, equations (7) and (8), we get the following eigenvalue problem:

$$\begin{bmatrix} \mathbf{X}(s)\mathbf{A}(s) \\ \mathbf{N}(s) \end{bmatrix} \mathbf{v}_1(s) = \begin{bmatrix} 0 \\ 0 \\ 0 \\ 0 \end{bmatrix} \quad \Rightarrow \quad \left| \begin{matrix} \mathbf{X}(s)\mathbf{A}(s) \\ \mathbf{N}(s) \end{matrix} \right| = 0 \qquad (11)$$

This relationship can be used to determine the stability of the system using a Nyquist contour around the entire right half plane (Bonnaure, 1991) or using a numeric search to solve for the eigenvalue locations (Hendricks et al, 1993). This numeric search requires starting with different initial guesses to converge to different eigenvalues. This can be a tedious procedure to make sure no important eigenvalues are missed. However, with an approximation to the system, utilizing rational polynomial functions instead of transcendental functions of the Laplace variable s, all of the dominant eigenvalues are determined by the eigenvalues of a single constant-coefficient matrix. A rational-polynomial approximation is useful for many other reasons, as described below.

2.4 Discussion

The model presented thus far is a modified version of that presented by Bonnaure (1991). The primary application of this form of model is stability calculations, which can be used to understand the importance of various design parameters on compressor operating range and stall inception behavior (Hendricks et al., 1993). For control law configuration and design, however, additional modifications are necessary.

Foremost is the necessity to transform the model from a homogeneous model to an input-output model. An input-output model describes *both* the homogeneous behavior (when the input is zero), and the effect of actuator motion. Such a model is necessary to incorporate the effects of feedback on the system stability. The addition of sensing and actuation to the model is presented below, and results in open loop transfer functions for each Fourier harmonic of a given compressor.

Once an input-output form is found, one can evaluate the effects of feedback in a systematic way. For control law *design*, however, an additional modification is highly desirable. Modern control design procedures utilize state space descriptions, or equivalently, rational-polynomial based transfer functions. In Section 3 we will see that the input-output model which results from direct application of the fluid relations above contains transcendental (rather than polynomial) functions of the frequency parameter s, and thus cannot be represented using a finite number of states. To alleviate this difficulty, we will derive an approximation of the fluid-dynamic transfer function (or 'truth model'). In Section 4 we will show that the approximate model is both an accurate representation of the flow physics of the truth model, and a useful form for control theoretic studies. The relative simplicity of the approximate model also makes it useful for system identification studies, which have proven to be important in rotating stall control research (Paduano et al., 1993, Haynes et al. 1993).

3 CONTROL THEORETIC MODIFICATIONS

This section presents the modifications motivated by the preceding discussion. In Section 3.1, an input-output model is developed, for a specific choice of sensor and actuator type. This model is infinite dimensional, and completely captures the dynamics represented by the fluid dynamic equations (1) and (3) with boundary conditions (5) and (6) and end conditions (7) and (8). This is our truth model for comparison with approximate models, and for ultimate evaluation of control system designs. In Section 3.2 the approximations are discussed. Section 4 verifies and applies the resulting approximate model.

3.1 Input-Output Model

To obtain an input-output (transfer function) model, one must choose the type and location of the actuation (inputs) and the sensors (outputs). For actuation we have chosen injection of high-momentum air, because it is predicted to be effective in controlling rotating stall (Hendricks and Gysling, 1992), and it is being implemented in current active control research compressors (see Figure 1 for a schematic: a high-speed valve modulates the mass flow injected from a high pressure source). For sensing (outputs), we have chosen static pressure, which is currently the most commonly sensed unsteady variable in high speed compressors. The (injected mass)-to-(static-pressure) transfer function is derived below, where actuator and sensor positions will be restricted to the inter-blade row gaps and the up- and down-stream ducts.

The effect of a jet actuator at axial location x_a in gap number ka can be described by:

$$\begin{aligned} \mathbf{J}_{ka}\mathbf{V}_{ka}(x_a,s)\mathbf{v}_{ka,downstream}(s) = \\ \mathbf{J}_{ka}\mathbf{V}_{ka}(x_a,s)\mathbf{v}_{ka,upstream}(s) + \mathbf{b}_{ka}u(s) \end{aligned} \qquad (12)$$

where the matrices $\mathbf{J}_{ka}$ and $\mathbf{b}_{ka}$ are the result of linearizing continuity, total temperature, and axial and circumferential momentum across an actuator disk at the air jet injection point. u is the control variable, in this case the ratio of injected mass flow to mean mass flow. A static pressure sensor at axial location x_s in gap number ks can be described by:

$$\frac{\delta P}{P}(s) = \mathbf{S}_{ks}\mathbf{V}_{ks}(x_s,s)\mathbf{v}_{ks}(s) \qquad (13)$$

where $\mathbf{S}_{ks}$ in this case is a row vector which simply selects the first element of $\mathbf{V}_{ks}(x_s,s)\mathbf{v}_{ks}(s)$, the static pressure solution from equation (4). Combining the actuator in the stacking process and solving for the sensor outputs, we arrive at the following relation:

$$\begin{aligned} \frac{\delta P}{P} = &\left(\mathbf{S}_{ks}\mathbf{V}_{ks}(x_s,s)\right)\cdot \\ &\left(\mathbf{A}_s(s)\begin{bmatrix} \mathbf{X}(s)\mathbf{A}(s) \\ \mathbf{N}(s) \end{bmatrix}^{-1}\begin{bmatrix} -\mathbf{X}(s)\mathbf{A}_a(s) \\ 0 \end{bmatrix} + \mathbf{A}_{as}(s)\right)\cdot \\ &\left(\mathbf{J}_{ka}\mathbf{V}_{ka}(x_a,s)\right)^{-1}\mathbf{b}_{ka}u_{ka}(s) \end{aligned} \qquad (14)$$

where $\mathbf{A}_s(s) = \mathbf{A}_{ks-1}(s)\cdots\mathbf{A}_1(s)$ is the stacked solution from the inlet to the sensor, $\mathbf{A}_a(s) = \mathbf{A}_K(s)\cdots\mathbf{A}_{ka}(s)$ is the stacked

solution from the actuator to the exit, and $\mathbf{A}_{as}(s)=\mathbf{A}_{ks-1}(s)\cdots\mathbf{A}_{ka}(s)$ is the stacked solution from the actuator to the sensor, or zero if the sensor is upstream of the actuator. Note that the matrix inverse is singular only at the eigenvalues of the system (equation 11), which now appear as poles in our transfer function, equation (14), which is our truth model.

3.2 Rational Approximation of Compressible Input-Output ('Truth') Model

In this section, several of the important relationships used by the model are approximated by finite-order polynomial transfer functions. This allows the overall system to be converted to a rational approximation, or equivalently, a state-space representation, for use in control law analysis and design.

The transcendental functions to be approximated in the blade row solutions, equation (1), are the functions $e^{\tilde{\alpha}_n(s)x}$, $e^{\tilde{\beta}_n(s)x}$, and $e^{\tilde{\chi}_n(s)x}$. At the blade row boundaries, x is known, so the only unknown is the Laplace variable s (equivalently, the time part of the solution). For instance, $e^{\tilde{\alpha}_n(s)x}$ can be written as:

$$\exp\left[\frac{x}{\cos\xi}\left(-\frac{jn}{r}\sin\xi+\frac{jn\Omega}{a-W}\right)\right]\cdot\exp\left(\frac{x}{(a-W)\cos\xi}\cdot s\right).$$

Once all of the known values are evaluated, this expression is simply a complex constant times $e^{-\tau s}$, the Laplace transform of a time delay τ, which can be approximated to an arbitrary degree of accuracy using a polynomial transfer function, usually a Padé approximation (Truxal, 1958):

$$e^{-\tau s}\approx\frac{1-a_1(\tau s)+a_2(\tau s)^2-\cdots\pm a_q(\tau s)^q}{1+a_1(\tau s)+a_2(\tau s)^2+\cdots+a_q(\tau s)^q}. \qquad (15)$$

Accuracy increases as the number of poles and zeros, q, increases, at the expense of increased model order and complexity. For the frequency range that is of interest for control law design of the first and second spatial harmonic, q=2 yields acceptable accuracy (see Section 4.1 for details). The characteristic frequency for mode number n is Ωn, so higher order Padé approximations might be necessary to approximate higher harmonics.

The total pressure and deviation lags are already in rational polynomial form, so the next step in the approximation is to eliminate inter-blade row gaps. eliminating gaps simplifies the system equations dramatically, and is valid in compressors with gaps that are short compared to the blade rows. To minimize the error introduced by this approximation, the blade rows are extended to account for the missing gap lengths. The boundary conditions for the model without gaps must of course be modified, and are as follows:

$$\mathbf{B}_k(x_{LEk},s)\tilde{\mathbf{v}}_k(s)=\mathbf{B}_{Lk}^{-1}\left(\mathbf{V}_{Lk}+\frac{1}{1+s\tau}\mathbf{P}_k\right)\mathbf{V}_{Tk}^{-1}\cdot\begin{pmatrix}\mathbf{B}_{Tk-1}\mathbf{B}_{k-1}(x_{TEk-1},s)\tilde{\mathbf{v}}_{k-1}(s)-\\ \frac{1}{1+s\tau}\mathbf{D}_{k-1}\mathbf{V}_{k-1}(x_{LEk-1},s)\mathbf{v}_{k-1}(s)\end{pmatrix} \qquad (16)$$

Notice that the relationship between $\mathbf{B}_{k-1}(x_{TEk-1},s)\tilde{\mathbf{v}}_{k-1}$ and $\mathbf{B}_k(x_{LEk},s)\tilde{\mathbf{v}}_k$ is a rational polynomial. The term involving the gap k-1 solution, $\mathbf{V}_{k-1}(x_{LEk-1},s)\mathbf{v}_{k-1}$, is due to the recursive nature of equation (6). It can be solved in terms of all the preceding blade row solutions and the inlet duct solutions which will be approximated presently.

By assuming infinitesimal gaps, the interconnection diagram in Figure 2 is simplified by replacing the frequency dependence of the gap solution with a constant transformation. In other words, the static pressure, density, and axial and circumferential velocities are now constant across the gap.

The final step in the approximation process is to combine the end conditions (7) and (8) with their respective boundary conditions (5) and (6), write the resulting transfer functions as ratios of analytic functions, and approximate these functions as polynomials using Taylor series expansions. For example, the exit condition, equation (8), combined with the trailing edge boundary condition for the last blade row, equation (6), can be written as:

$$\mathbf{X}(s)\mathbf{v}_{K+1}(s)=\mathbf{X}(s)\left(\mathbf{V}_{TK+1}\mathbf{V}_{K+1}(x_{TEK},s)\right)^{-1}\cdot\begin{pmatrix}\mathbf{B}_{TK}\mathbf{B}_K(x_{TEK},s)\tilde{\mathbf{v}}_K(s)-\\ \frac{1}{1+s\tau}\mathbf{D}_K\mathbf{V}_K(x_{LEK},s)\mathbf{v}_K(s)\end{pmatrix}=0 \qquad (17)$$

Solving (17) for $\tilde{B}_K$, the magnitude of the upstream traveling pressure perturbation in the last blade row, in terms of the other variables leads to the transfer functions $\tilde{B}_K/\tilde{C}_K$, $\tilde{B}_K/\tilde{E}_K$, $\tilde{B}_K/\delta\beta_K$. Each of these must be approximated by a polynomial transfer function. For example, $\tilde{B}_K/\tilde{C}_K$ is:

$$\frac{\tilde{B}_K(s)}{\tilde{C}_K(s)}=\frac{d_c\cosh(a\sqrt{y(s)})+g_c(s)\dfrac{\sinh(a\sqrt{y(s)})}{\sqrt{y(s)}}}{d_b\cosh(a\sqrt{y(s)})+g_b(s)\dfrac{\sinh(a\sqrt{y(s)})}{\sqrt{y(s)}}} \qquad (18)$$

where d_b, d_c and a are constants, g_b and g_c are polynomials in s, and

$$a=\frac{1}{1-M_x^2}\frac{\Delta x}{r}$$

$$y(s)=n^2(1-M_x^2)+\left(\frac{sr}{a}+jnM_\theta\right)^2$$

Using Taylor series in the numerator and the denominator, one

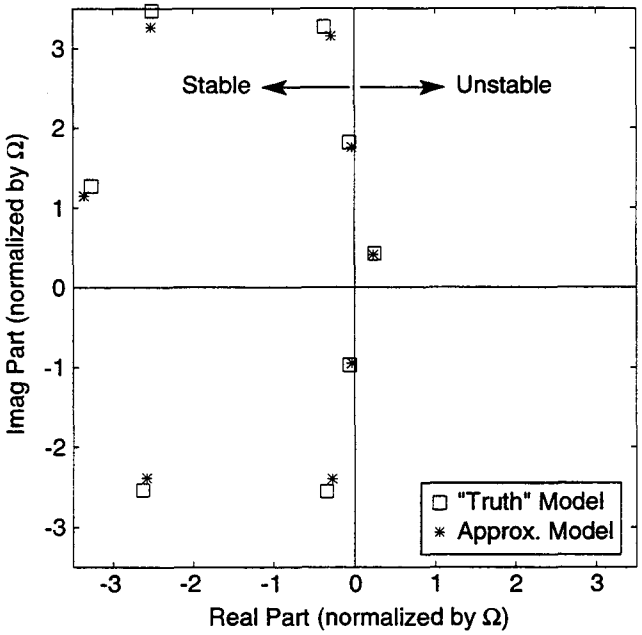

Figure 3 - Eigenvalue comparison between 'truth' and approximate models.

can derive a rational polynomial approximation for this equation:

$$\frac{\tilde{B}_K(s)}{\tilde{C}_K(s)} \approx \frac{b_0 + b_1 s + b_2 s^2 + \cdots}{c_0 + c_1 s + c_2 s^2 + \cdots}$$

Approximating all of the relevant transfer functions in this way leads to a standard control form for the input-output dynamics.

4 APPLICATION OF CONTROL MODEL

In this section, we apply our control modeling and approximation techniques to a 3-stage high speed axial compressor geometry. The inputs to the procedure are the blade chords and staggers, the inlet and exit duct geometry, the mean flow conditions, and the individual blade row characteristics (pressure rise, loss, and deviation coefficients). All of these parameters were chosen to match, as closely as possible, an industrial high-speed three-stage compressor test facility.

After verifying that the control model characteristics are close approximations to the 'truth' model characteristics (Section 4.1), we will turn our attention to the important question of sensor and actuator placement for feedback stabilization (Section 4.2). The primary purpose here is to demonstrate the capability provided by the control theoretic model, but we also intend to demonstrate the importance of careful choice of actuator location, sensor location, and sensor type. A method for making such choices is also developed below.

4.1 Accuracy of the Approximate Model

As a first check on the accuracy of our approximation, we

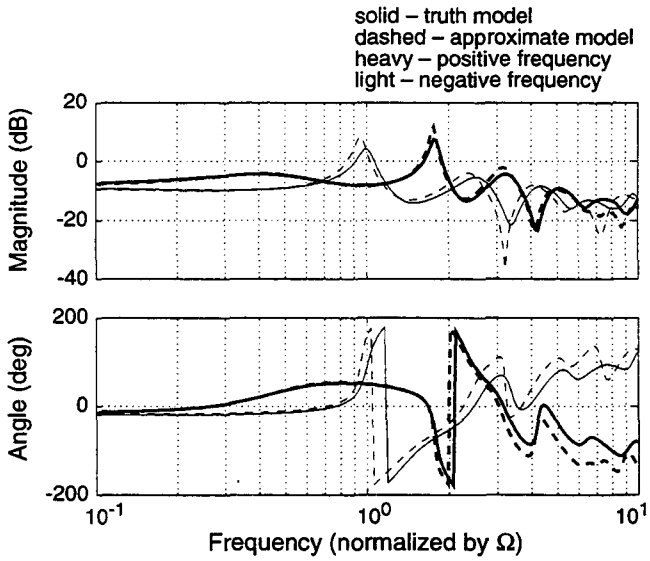

Figure 4 - Frequency reponse comparison between truth model and approximate model for positive and negative frequencies.

can test whether its homogeneous response characteristics match those of the truth model. Similarity of the homogeneous response can be insured up to some maximum frequency by comparing the eigenvalues of the two systems up to that frequency[2]. If all of the eigenvalues are the same or similar, then the low-frequency homogeneous response characteristics will be comparable. Figure 3 shows this eigenvalue comparison, which confirms that the eigenvalue locations are nearly identical for low frequencies. At higher frequencies (>2Ω) the approximate eigenvalues begin to lose accuracy, but as we will see, the difference exhibited does not have a severe adverse effect on the input-output response characteristics until well beyond 3Ω.

A more complete test of the accuracy of the approximation is to look at the forced response characteristic, or Bode plot, as a function of frequency. Such a plot incorporates both the homogeneous effects and the effects of forcing. From standard control theory (Saucedo and Shiring, 1968), we know that a control law design will remain stable if the actual model to which it is applied is not too much different than the model used for design. Typical designs exhibit more than 6 dB in gain margin and 40 degrees in phase margin; this fact provides us with a rough rule of thumb for comparing the approximate model to the truth model: if the approximate model does not differ from the truth model by more than 3 dB in magnitude, and 20 degrees in phase, then the model is useful for the purpose of robust controller design (especially if the truth model is used for final design validation).

Figure 4 shows a Bode plot (containing both positive and negative frequency responses) comparison of the truth model and the rational-approximate model with the actuator in gap 2

[2] The desired accurate frequency range will be determined by many factors, including the bandwidth of the controller, the level of instability and frequency of the unstable eigenvalues, and the actuator dynamics.

(after the first blade row) and the sensor in gap 1 (the inlet duct). Figure 4 shows a maximum difference of less than 1 dB in gain and 5 degrees in phase for frequencies $<\Omega$ (rotating stall typically occurs at about one-half Ω). Therefore, the error in modeling is small compared to the desired robustness bounds in this region, and does not exceed our 3 dB/20 degree criterion until well above 3Ω.

4.2 Sensor-Actuator Placement

In this section, we briefly explore the important question of sensor and actuator placement, using the rational approximate model derived above. We will show that, in this compressor, some sensor and actuator locations are much more desirable than others. We will also see that the model is useful for sorting through the large number of options that exist, and for verifying that the best locations obtained are 'robust' to variations in the input parameters, the operating conditions, and the modes to be stabilized.

In order to sort through the many combinations of actuator and sensor positions available, a performance metric must be adopted. Typically, one chooses a measure of optimality that reflects both the size of the perturbations which occur in the controlled system, and the amount of control activity required to achieve stabilization (one might also choose range extension as a performance measure, but this typically leads to nonlinear considerations, which are outside the scope of this study). A trade-off exists between control activity reduction and perturbation magnitude reduction, so one must weight the importance of each. Also, some measure of the level of excitation and measurement noise inherent in the physical system must be provided.

Once a good set of sensor and actuator locations has been identified, it is necessary to determine the sensitivity of the result to the assumptions made. For example, the set chosen must be nearly optimal for different operating conditions, and its relative performance must not be too sensitive to the input parameters (such as the blade pressure rise, loss, and deviation characteristics). Since we expect to stabilize the second and perhaps the third circumferential harmonic as well as the first, we also want to choose actuator and sensor locations that are effective for these harmonics. The sensor and actuator location choice is 'robust' if it remains desirable under all of these variations -- stage characteristic variations, operating condition changes, and harmonics stabilized.

4.2.1 Procedure. Linear Quadratic-Gaussian (LQG) optimal control techniques will be used to measure optimality of sensor and actuator locations. LQG optimal control minimizes the mean square of a combination of control and state activity. LQG optimal controllers are known to have poor robustness to plant parameter uncertainty, so we do not expect the control law designs to be especially attractive for implementation. Solving the LQG problem does, however, allow one to determine the 'best possible performance' (without regard for parameter robustness) that a given sensor/actuator pair can achieve, in the form of the LQG performance index. As such the so-called 'LQG cost' is a rigorous, mean-square type measure for comparing sensor/actuator location pairs. Once a good combination has been identified, robustness issues can be taken into account in a second control law design iteration by using, for instance, a μ-synthesis design technique (Doyle, 1983).

The first step in the procedure is to write the input-output system for a particular harmonic as a vector-matrix differential equation:

$$\begin{aligned} \dot{\mathbf{x}} &= \mathbf{F}\mathbf{x} + \mathbf{G}u + \xi \\ \frac{\delta P}{P} &= \mathbf{H}\mathbf{x} + \mathbf{D}u + \varsigma \end{aligned} \tag{19}$$

where $\mathbf{x}$ is a vector of internal states (including pressure and velocity modes which are not measured), and $\mathbf{F}$, $\mathbf{G}$, $\mathbf{H}$ and $\mathbf{D}$ result from the frequency-domain to state-space conversion of the rational approximate model. Such conversion is easily accomplished for any rational-polynomial transfer function (Reid, 1983). ξ and ζ are disturbance excitations, which are considered to be white noise with covariance $\mathbf{Q}$ and $\mathbf{R}$ respectively.

Using this state-space description, we can formulate and solve the standard LQG optimal control problem (Bryson and Ho, 1975). A performance index J, over a time interval t_o to t_f, can be written:

$$J = E\left\{\frac{1}{2}\int_{t_0}^{t_f}\left(\mathbf{x}^T\mathbf{A}\mathbf{x}+\mathbf{u}^T\mathbf{B}\mathbf{u}\right)dt\right\} \tag{20}$$

where E is the expected value, and $\mathbf{A}$ and $\mathbf{B}$ are weighting matrices chosen by the designer (usually diagonal). J measures the *weighted mean-square state deviation* ($\int \mathbf{x}^T\mathbf{A}\mathbf{x}$ - this could, for instance, be chosen to measure static pressure deviations), plus *the weighted mean-square actuator activity* ($\int \mathbf{u}^T\mathbf{B}\mathbf{u}$), associated with stabilizing the system (19). The solution to this optimization problem is beyond the scope of this paper, but the resulting minimum can be calculated, for t_f-t_o approaching infinity (steady state solution, *SS*), as:

$$J_{min}^{SS} = Tr\left\{\mathbf{S}\mathbf{Q}+\mathbf{C}^T\mathbf{B}\mathbf{C}\mathbf{P}\right\} \tag{21}$$

where Tr is the trace, $\mathbf{C[B, G, S]}$ is the optimal regulator gain, $\mathbf{S[A, B, F, G]}$ is the solution to the control Riccati equation, and $\mathbf{P[F, H, Q, R]}$ is the solution to the estimation Riccati equation (Bryson and Ho, 1975). Equation (21) can be used to compare different sensor and actuator location pairs, multiple sensors and actuators, different sensor types, but not different actuator types directly since different actuators will require different weightings in equation (20).

The procedure described above is complicated by the necessity to select state and control weightings ($\mathbf{A}$ and $\mathbf{B}$) and noise covariance matrices ($\mathbf{Q}$ and $\mathbf{R}$). $\mathbf{A}$ and $\mathbf{B}$ weight the relative importance of actuator motion and, for instance, mean square pressure fluctuations (which are modeled by $E\left\{\int_{t_0}^{t_f}\mathbf{x}^T\mathbf{A}\mathbf{x}dt\right\}$). $\mathbf{Q}$ and $\mathbf{R}$ model the size, location, and type of disturbances entering the system. Since little engineering data exists on the relative sizes of these terms, we will attempt to

Table I: LQG cost, J_{min}^{SS}, Nominal Case

		Sensor Location (Figure 1 gap numbering scheme)							
		1	2	3	4	5	6	7	8
	1	2.05	3.67	4.12	5.56	5.53	10.06	9.22	2.37
	2	0.93	1.66	1.87	2.52	2.50	4.55	4.17	1.07
Actuator	3	1.20	2.14	2.41	3.24	3.23	5.87	5.38	1.38
Location	4	2.61	4.68	5.25	7.08	7.04	12.81	11.74	3.01
(cf. Fig 1)	5	3.12	5.60	6.28	8.48	8.43	15.34	14.06	3.61
	6	15.32	27.45	30.80	41.54	41.33	75.19	68.91	17.69
	7	9.19	16.46	18.46	24.90	24.78	45.08	41.31	10.60
	8	119.28	213.71	239.75	323.39	321.77	585.52	536.62	137.69

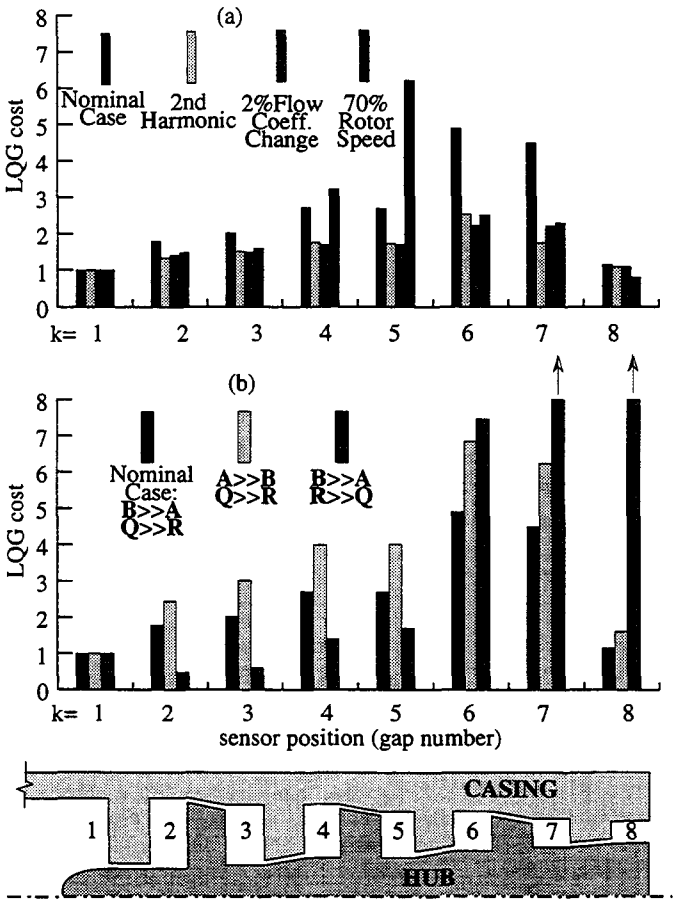

Figure 5 - Sensitivity of LQG cost to changes in test conditions. Results are normalized against station 1 costs. Actuator is at located in gap #2.

'bracket' the possibilities by testing several cases involving relative extremes. For instance, it is desired to have small control action so as not to saturate the jet actuator and not to recirculate too much air. It is also desired to have small state perturbations, since large perturbations lead to nonlinear behavior. To see how this trade-off effects the choice of sensor and actuator locations, we perform the optimization both with actuator motion heavily weighted with respect to state perturbations (**B>>A**), and vice versa.

4.2.2 Results. Our nominal case is as follows: the control weighting matrix **B** is chosen to be much higher than the state weighting. Both weighting matrices **A** and **B** are in the form of a constant multiplied by an identity matrix ($\mathbf{A}=\alpha\mathbf{I_A}$ and $\mathbf{B}=\beta\mathbf{I_B}$), i.e. no cross-weighting terms. The state process noise ξ is applied to the total pressure loss equation for each blade row with equal independent variance. The sensor noise ζ is chosen to be much smaller than the process noise with zero cross correlation (i.e. **Q** and **R** diagonal, **Q>>R**).

The nominal compressor operating conditions are for 100% design speed at a flow coefficient of .4506 - this corresponds to the eigenvalue locations and frequency response plots in Figures 3 and 4. Table I shows the costs for all of the sensor/actuator location pairs.

Table I clearly shows the necessity for careful choice of sensor and actuator location. For instance, placing the actuators upstream of the compressor (gap #1) yields good performance, but a factor of two improvement in the mean squared actuator motion required can be achieved by moving the actuators downstream of the inlet guide vanes (IGVs). Also note that collocation of actuators and sensors is not necessarily the best choice.

To check the sensitivity of our results to variations in the test conditions, we compare the variation of cost with sensor location for various cases. In each case, we use actuator location #2 because, based on tables such as Table I, this appears to be the best location regardless of the test conditions. In Figure 5a, we compare the nominal case to various other cases: stabilization of the second harmonic instead of the first, stabilization at a different flow coefficient, and a stabilization at a different rotor speed. LQG costs are normalized to 1 at the front of the compressor (gap #1) to compare trends when using different assumptions. The absolute magnitudes are not important in this comparison. We conclude based on Figure 5a that under all of the variations mentioned, sensor locations near the front of the compressor or in the downstream gap are consistently the best choices, and are therefore considered 'robust' choices for the sensor location.

In Figure 5b we demonstrate the insensitivity of the results to the choice of the weighting matrices **A** and **B**, as well as the noise covariance matrices **Q** and **R**. Again, the costs are normalized to 1 at gap #1. Based on Figure 5b we conclude that, although a trade-off exists between actuator activity and

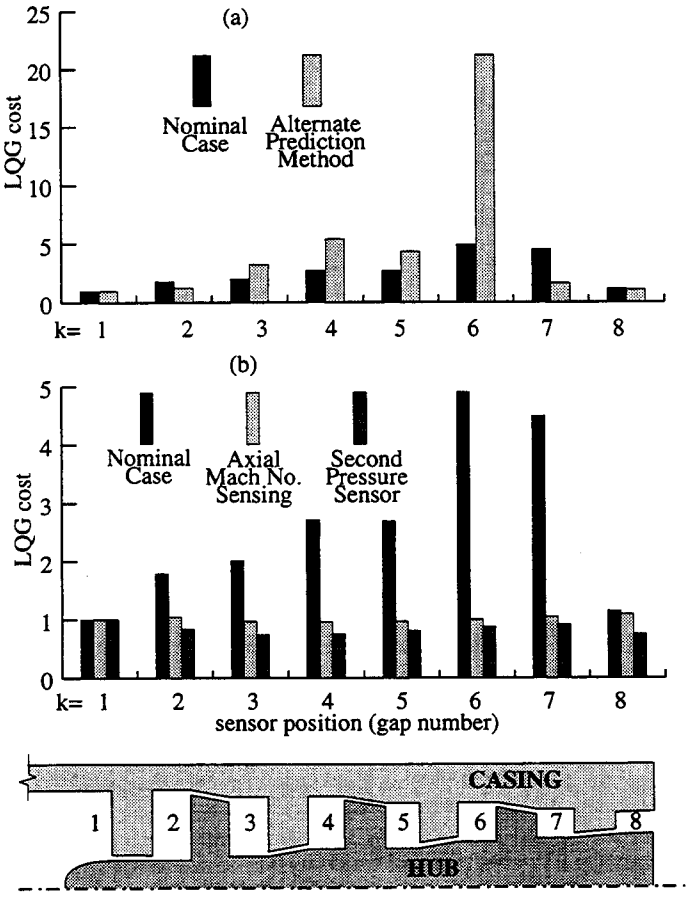

Figure 6 - Sensitivity of LQG cost to changes in test conditions. In (a), all costs are normalized against station 1 costs. In (b), costs are normalized against nominal station 1 cost. Actuator is at location 2 for all cases.

mean squared perturbation amplitudes, this trade-off does not (in this case) strongly affect the choice of where to put the sensors. More detailed study of tables such as Table I indicates that the actuator location is similarly robust to the LQG cost weightings.

Figure 6a shows the effect on the cost of changing the mean-flow prediction method, again with costs normalized to 1 at gap #1. In the nominal case, stage characteristics supplied by the manufacturer were utilized, while in the second case, correlations (described in Hendricks et al., 1993) were utilized. Here strong variations in the costs are seen at some axial stations, demonstrating that the individual stage characteristics can have a strong effect on the behavior of the controlled system. Nevertheless, sensor locations near the front or the back of the compressor are still the most desirable, and studies not presented here indicate that actuator location choices are similarly robust.

Finally, it is of interest to look at various options for the sensor configuration. We have used static pressure sensing for our comparisons, because such sensing is relatively standard in modern high-speed compressor tests. If a different sensor type is determined to be much more attractive for active control, however, it may be desirable to develop new sensors specifically for active control. Further, we would like to know whether sensing at additional locations (i.e. at two rather than one axial station) has significant benefit. Figure 6b compares the nominal LQG costs to the costs if (1) axial velocity is sensed instead of static pressure, and (2) static pressure is measured at station 1, and an *additional sensor array* is placed at another axial station. Figure 6b is normalized by the nominal gap #1 results rather than the individual gap #1 results, since in this case all the assumptions are the same and the magnitudes of the costs *between* cases is important.

The most notable difference seen in Figure 6b between pressure and axial Mach number sensing is that axial Mach number sensing is much less sensitive to axial location than pressure sensing. This may be an important advantage during the experimental stages of stall control testing, and agrees with the general conclusion by Hendricks et al. that perturbation mass flow amplitudes are nearly uniform along the compressor, even in the case of compressible flow. Note also in Figure 6b that a second static pressure sensor can lower the best cost by an additional 25%.

It is not known whether the results in Figures 5 and 6 have more general implications for the behavior of actively controlled high speed compressors. It is clear, however, that efforts in active control should rely on as much knowledge of the compressor dynamics as possible, because the effects on the overall performance of the controller can be highly dependent on these dynamics. The modeling and evaluation procedures presented here are a first step toward a rigorous approach to the design of active control systems for high-speed axial compressors.

5 SUMMARY AND CONCLUSIONS

A two-dimensional, compressible model of axial compressor dynamics has been extended to include the effects of the inlet and exit conditions of finite length ducts resulting in a new eigenvalue problem. This analytical model has been manipulated into an input-output form suitable for control analysis and design. By applying transcendental-to-rational transfer function approximation procedures, and by approximating the inter-blade row gaps as extensions of their adjacent blade rows, an approximate, finite dimensional, control-theoretical model has been derived. The resulting model is accurate in the region of the instability in the Laplace domain, which allows one to use the approximation model to deduce behavior of the analytical model.

The state-space form of the approximate model was used with the LQG performance index to identify LQG optimal axial locations for the sensors and actuators. The resulting optimal locations were found to be good for different harmonics, and were also insensitive to changes in operating conditions. The addition of a second static pressure sensor resulted in a lower (better) performance index. Finally, a comparison between axial velocity sensing and a static pressure sensing showed that axial velocity sensing yields slightly better performance and is less sensitive to axial placement.

Future modeling work will include modeling the inter-blade row gap equations in the rational approximate model. Approximating the gap equations directly will yield a state-space model which is even more accurate. Future control design

work will include an μ–synthesis design procedure (Doyle, 1983) to increase stability robustness while still incorporating performance criteria.

6 ACKNOWLEDGMENTS

This work was supported by the US Air Force Office of Scientific Research, James A. Fein, technical monitor. M. Feulner is supported by the Draper Laboratory Fellowship program. This support is gratefully acknowledged.

REFERENCES

Adomaitis, R. A., and Abed, E. H., "Local Nonlinear Control of Stall Inception in Axial Flow Compressors," AIAA Paper #93-2230, Presented at the 29th Joint Propulsion Conference, June 28-30, 1993, Monterey, CA.

Badmus, O. O., Chowdhury, S., Eveker, K. M., Nett., C. N., and Rivera, C. J., "A Simplified Approach for Control of Rotating Stall, Parts I and II", AIAA Papers 93-2229 and 93-2234, Presented at the 29th Joint Propulsion Conference, June 28-30, 1993, Monterey, CA.

Bonnaure, L. P., 1991, "Modelling High Speed Multistage Compressor Stability," Masters Thesis, Massachusetts Institute of Technology, Cambridge, MA.

Bryson, A. E. and Ho, Y.-C., 1975, *Applied Optimal Control*, Hemisphere Publishing Corp., New York.

Doyle, J. C., "Synthesis of Robust Controllers and Filters," Proc. IEEE Conf. on Decision and Control, San Antonio, TX, 1983, pp. 109-114.

Epstein, A. H., Ffowcs-Williams, J. E., and Greitzer, E. M., "Active Suppression of Aerodynamic Instabilities in Turbomachines," AIAA Paper 86-1994. Also *Journal of Propulsion*, 1989, Vol. 5, No. 2, pp. 204-211.

Ffowcs Williams, F. E., and Huang, X., "Active Stabilization of Compressor Surge," *Journal of Fluid Mechanics,* vol. 204, 1989, pp. 245-262.

Greitzer, E. M., "Surge and Rotating Stall in Axial Flow Compressors, Part I: Theoretical Compression System Model, and Part II: Experimental Results and Comparison with Theory," *ASME Journal of Engineering for Power,* Vol. 98, no. 2, April, 1976, pp. 190-216.

Greitzer, E. M., Epstein, A. H., Guenette, G. R., Gysling, D. L., Haynes, J., Hendricks, G. J., Paduano, J. D., Simon, J. S., and Valavani, L., "Dynamic Control of Aerodynamic Instabilities in Gas Turbine Engines," AGARD Lecture Series 183, *Steady and Transient Performance Prediction of Gas Turbine Engines,* AGARD-LS-183, May 1992.

Haynes, J. M., Hendricks, G. J., and Epstein, A. H., "Active Stabilization of Rotating Stall in a Three-Stage Axial Compressor," ASME Paper #93-GT-346, presented at the International Gas Turbine and Aeroengine Congress and Exposition, Cincinnati, Ohio, May 24-27, 1993.

Hendricks, G. J., and Gysling, D. L., "A Theoretical Study of Sensor-Actuator Schemes for Rotating Stall Control," presented at the AIAA/SAE/ASME/ASEE 28th Joint Propulsion Conference and Exhibit, Nashville, TN, 1992

Hendricks, G. J., Bonnaure, L. P., Longley, J. P., Greitzer E. M., Epstein A. H., "Analysis of Rotating Stall Onset In High-Speed Axial Flow Compressors," AIAA paper 93-2233, Presented at the 29th Joint Propulsion Conference, June 28-30, 1993, Monterey, CA.

Longley, J. P., "A Review of Non-Steady Flow Models for Compressor Stability," ASME Paper 93-GT-17, presented at the International Gas Turbine and Aeroengine Congress and Exposition, Cincinnati, Ohio, May 24-27, 1993.

Mansoux, C., Gysling, D. L., and Paduano J. D., "Distributed Nonlinear Modeling and Stability Analysis of Axial Compressor Stall and Surge," to appear, proceedings of the 1994 American Control Conference, June 29, 1994, Baltimore.

McCaughan, F. E., "Application of Bifurcation Theory to Axial Flow Compressor Stability," *ASME Journal of Turbomachinery*, Vol. 3, October 1989a, pp. 426-433.

McCaughan, F. E., "An Analytical and Numerical Study of Axial Flow Compressor Instability," *ASME Journal of Turbomahinery*, Vol. 3, October 1989b, pp. 434-441.

Moore, F. K. and Greitzer, E. M., "A Theory of Post-Stall Transients in Axial Compression Systems, Part I - Development of Equations, and Part II - Application, " *ASME Journal of Engineering for Gas Turbines and Power,* Vol. 108, 1986, pp. 68-97.

Paduano, J. D., Valavani, L., Epstein, A. H., and Greitzer, E. M., "Modeling for Control of Rotating Stall," IEEE 29th Conference on Decision and Control, December 1990 (to appear, *Automatica,* Vol. 30, No. 9, September 1994).

Paduano, J. D., Epstein, A. H., Valavani, L., Longley, J. P., Greitzer, E. M., and Guenette, G. R., "Active Control of Rotating Stall in a Low-Speed Axial Compressor" *Journal of Turbomachinery*, Vol. 115, January 1993, pp. 48-56.

Paduano, J. D., Valavani, L., and Epstein, A. H., "Parameter Identification of Compressor Dynamics During Closed-Loop Operation," *Journal of Dynamic Systems, Measurement, and Control*, December 1993.

Pinsley, J. E., Guenette, G. R., Epstein, A. H., and Greitzer, E. M., "Active Stabilization of Centrifugal Compressor Surge," *Journal of Turbomachinery*, vol. 113, 1991, pp. 723-732.

Reid, J. G., *Linear System Fundamentals*, McGraw Hill, 1983.

Saucedo, R., and Shiring, E. E., *Introduction to Continuous and Digital Control Systems,* Macmillan, New York, 1968.

Takahashi, Y., Rabins, M. J., and Auslander, D. M., *Control of Dynamic Systems*, Addison-Wesley, 1972.

Truxal, *Control Engineers Handbook*, McGraw Hill, 1958.